Liquid Crystals
Publication details, including instructions for authors and subscription information:
http://www.informaworld.com/smpp/title~content=t713926090

Synthesis, structure and properties of new chiral liquid crystalline monomers and homopolysiloxanes containing menthyl groups

Jian-She Hu[a]; Ke-Qi Wei[a]; Bao-Yan Zhang[a]; Li-Qun Yang[a]
[a] Center for Molecular Science and Engineering, Northeastern University, Shenyang, People's Republic of China

To cite this Article Hu, Jian-She , Wei, Ke-Qi , Zhang, Bao-Yan and Yang, Li-Qun(2008) 'Synthesis, structure and properties of new chiral liquid crystalline monomers and homopolysiloxanes containing menthyl groups', Liquid Crystals, 35: 8, 925 — 935
To link to this Article: DOI: 10.1080/02678290802295729
URL: http://dx.doi.org/10.1080/02678290802295729

Liquid Crystals,
Vol. 35, No. 8, August 2008, 925–935

Taylor & Francis
Taylor & Francis Group

Synthesis, structure and properties of new chiral liquid crystalline monomers and homopolysiloxanes containing menthyl groups

Jian-She Hu, Ke-Qi Wei, Bao-Yan Zhang* and Li-Qun Yang

Center for Molecular Science and Engineering, Northeastern University, Shenyang, 110004, People's Republic of China

(Received 14 March 2008; final form 23 June 2008)

The synthesis is described of four new chiral liquid crystalline monomers ($\mathbf{M_2}$–$\mathbf{M_5}$) and their corresponding side-chain homopolysiloxanes ($\mathbf{P_2}$–$\mathbf{P_5}$) containing menthyl groups. Chemical structures were characterised using FT-IR or ^{1}H NMR spectra, and specific optical rotations were evaluated with a polarimeter. The phase behaviour and mesomorphic properties of the new compounds were investigated by differential scanning calorimetry, thermogravimetric analysis, polarising optical microscopy, UV/visible/NIR spectrocopy and X-ray diffraction. The monomers and homopolymers with more aryl segments showed noticeably lower specific optical rotation value. The monomers $\mathbf{M_2}$–$\mathbf{M_5}$ formed a cholesteric or blue phase when a flexible spacer was inserted between the rigid mesogenic core and the terminal menthyl groups by reducing the steric effect. $\mathbf{M_2}$–$\mathbf{M_5}$ revealed enantiotropic cholesteric phase. Moreover, $\mathbf{M_2}$ also exhibited a monotropic smectic A (SmA) phase, and $\mathbf{M_4}$ also exhibited a cubic blue phase on cooling. The selective reflection of light shifted to the long wavelength region with increasing rigidity of the mesogenic core for $\mathbf{M_2}$–$\mathbf{M_5}$. $\mathbf{P_2}$–$\mathbf{P_5}$ exhibited SmA phases, and the mesogenic moieties were ordered in smectic orientation with their centres of gravity in planes. Melting or glass transition temperature and the clearing temperature increased, and the mesophase temperature range widened with increasing rigidity of the mesogenic core.

Keywords: menthyl moiety; liquid crystalline polymer; cholesteric phase; smectic phase; blue phase

1. Introduction

Chiral liquid crystalline polymers (LCPs) have attracted much interest because of their unique optical and electrical properties, including the selective reflection of light, thermochromism, ferroelectricity and their potential applications as electro-optical materials (*1–12*). Chirality can be introduced into side-chain LCPs at various levels. They are located in the terminal position of the mesogenic units. The rod-like, chiral molecules responsible for the macroscopic alignment of the mesogenic domains can produce cholesteric, blue or chiral smectic C phases. Depending on the chemical structure, it may be feasible to achieve a macroscopic alignment of the chiral mesophase domains. In recent years, many side-chain chiral LCPs, mostly based on commercially available chiral compounds, such as cholesterol (*2, 6, 13, 14*) and (*S*)-(+)-2-methyl-1-butanol (*15–21*), have been studied.

Menthol derivatives have been used as a non-mesogenic chiral monomer for the synthesis of side-chain chiral LCPs (*22–32*). Bobrovsky *et al.* (*24–27*) reported detailed studies on copolymers based on methyl groups, but in these instances, smectic and cholesteric phases were induced by the introduction of non-mesogenic chiral menthyl monomer into nematic or smectic polymers. Liu and Yang (*31*) reported synthesis and characterisation of novel monomers and polymers containing chiral (–)-menthyl groups. Although these chiral monomers, containing two or three phenyl rings, had good rigidity and tended to exhibit a mesophase, their mesogenic cores were directly linked to terminal menthyl groups; thus the existence of the bulky steric menthyl groups prevented the development of the LC phase.

To date, to the best of our knowledge, the synthesis and characterisation of LC monomers and their homopolymers directly containing mesogenic menthyl groups have not been reported. We found that these monomers and their homopolymers containing menthyl groups could form and exhibit cholesteric, blue or smectic phases when a flexible spacer was inserted between the rigid mesogenic core and the bulky terminal menthyl fragments by reducing the steric effect. This is similar to the decoupling effects observed when a flexible spacer is inserted between the polymeric main chain and the mesogenic side groups. Therefore, it is necessary to design and synthesise novel chiral LC monomers and polymers derived from menthol to study their structure–property relationships and explore their potential applications. In this study, four new chiral LC monomers and their corresponding homopolysiloxanes based on menthyl groups were prepared and

*Corresponding author. Email: byzcong@163.com

ISSN 0267-8292 print/ISSN 1366-5855 online

DOI: 10.1080/02678290802295729
http://www.informaworld.com

characterised. Their mesomorphic properties and phase behaviour were investigated with differential scanning calorimetry (DSC), thermogravimetric analysis (TGA), polarising optical microscopy (POM), UV/visible/NIR spectroscopy and X-ray diffraction (XRD). The structure–property relationships of the monomers and homopolymers obtained are discussed.

2. Experimental

Materials

Menthol ($[\alpha]_D^{20} = -50.5^\circ$) was purchased from Shanghai Kabo Chemical Co. Chloroacetic acid was purchased from Tianjin Bodi Chemical Co. 4-Hydroxybenzoic acid was obtained from Shanghai Wulian Chemical Plant. Allyl bromide was purchased from Beijing Chemical Reagent Co. 4, 4′-Dihydroxybiphenyl (from Aldrich) was used as received. Polymethylhydrosiloxane (PMHS, $\bar{M}_n$= 700–800) was purchased from Jilin Chemical Industry Co. Toluene used in the hydrosilylation reaction was purified by treatment with $LiAlH_4$ and distilled before use. All other solvents and reagents used were purified by standard methods.

Measurements

FT-IR spectra were measured on a Perkin-Elmer Spectrum One (B) spectrometer. ^{1}H NMR spectra were obtained with a Bruker ARX400 spectrometer. The special optical rotations were obtained on a Perkin-Elmer 341 polarimeter. The selective reflection wavelength was measured with a Perkin-Elmer 950 UV/Vis/NIR spectrometer with hot stage. The phase behaviour was determined with a Netzsch DSC 204 equipped with a cooling system. The heating and cooling rates were $10^\circ C\,min^{-1}$. The thermal stability of the polymers under nitrogen atmosphere was measured with a Netzsch TGA 209C thermogravimetric analyser. The heating rates were $20^\circ C\,min^{-1}$. A Leica DMRX polarising optical microscope equipped with a Linkam THMSE-600 cool and hot stage was used to observe the phase transition temperatures and analyse the mesomorphic properties through the observation of optical textures. XRD measurements were performed with a nickel-filtered Cu-K_α (λ=1.542 Å) radiation with a DMAX-3A Rigaku powder diffractometer.

Synthesis of the intermediate compounds

The synthetic route of the intermediate compounds is outlined in Scheme 1. Yields, melting temperatures and IR characterisation of the main intermediate compounds are summarised in Table 1. Menthyloxyacetic acid (**1**), 4-allyloxybenzoic acid (**5**), 4-allyloxy-4′-hydroxybiphenyl (**6**) and 4-hydroxyphenyl-4′-allyloxybenzoate (**8**) were prepared according to the methods reported previously (*33–35*).

*4-Menthyloxyacetyloxybenzoic acid (**3**).*

Menthyloxyacetyl chloride **2** was prepared through the reaction of compound **1** with excess thionyl chloride according to a method similar to that reported in the literature (*13*). Compound **2** (23.3 g, 0.1 mol), dissolved in 30 ml of dry tetrahydrofuran (THF), was added dropwise to a solution of 4-hydroxybenzoic acid (13.8 g, 0.1 mol) in 200 ml of THF and 8 ml of pyridine. The mixture was reacted for 6 h at room temperature, and then 10 h at 60°C. After removing the solvent by rotatory evaporation, the residue was poured into a beaker filled with 800 ml of ice-water. The crude product, obtained by filtration, was washed several times with warm water, and then recrystallised from 80% ethanol. White solid **3** was obtained.

*4-Hydroxybiphenyl 4′-allyloxybenzoate (**9**).*

The synthesis of compound **9** was carried out using a method similar to that for compound **3**. 4-Allyloxybenzoyl chloride **7** (19.7 g, 0.1 mol) was dissolved in 50 ml of THF, and then added dropwise to a solution of 4,4′-dihydroxybiphenyl (55.9 g, 0.3 mol) in 350 ml of THF and 8 ml of pyridine. The mixture was reacted for 5 h at room temperature, and then refluxed for 12 h. After removing the solvent by rotatory evaporation, the residue was poured into a beaker filled with 500 ml of water. The crude product, obtained by filtration, was washed several times with 1% NaOH solution, neutralised with hydrochloric acid, washed with hot ethanol and then recrystallised from acetone. White solid **9** was obtained.

Synthesis of the monomers

The synthetic route of the vinyl monomers is shown in Scheme 2. The monomers $\mathbf{M_1}$–$\mathbf{M_5}$ were prepared by the same method. The synthesis of $\mathbf{M_1}$ is described below as an example.

*4-Allyloxybenzoyloxyphenyl 4′-menthyloxyacetate (**M$_1$**).*

Menthyloxyacetyl chloride **2** (11.7 g, 0.05 mol) was dissolved in 20 ml of dry chloroform, and then added dropwise to a solution of compound **8** (13.5 g, 0.05 mol) in 200 ml of chloroform and 15 ml of pyridine while stirring. The mixture was refluxed for

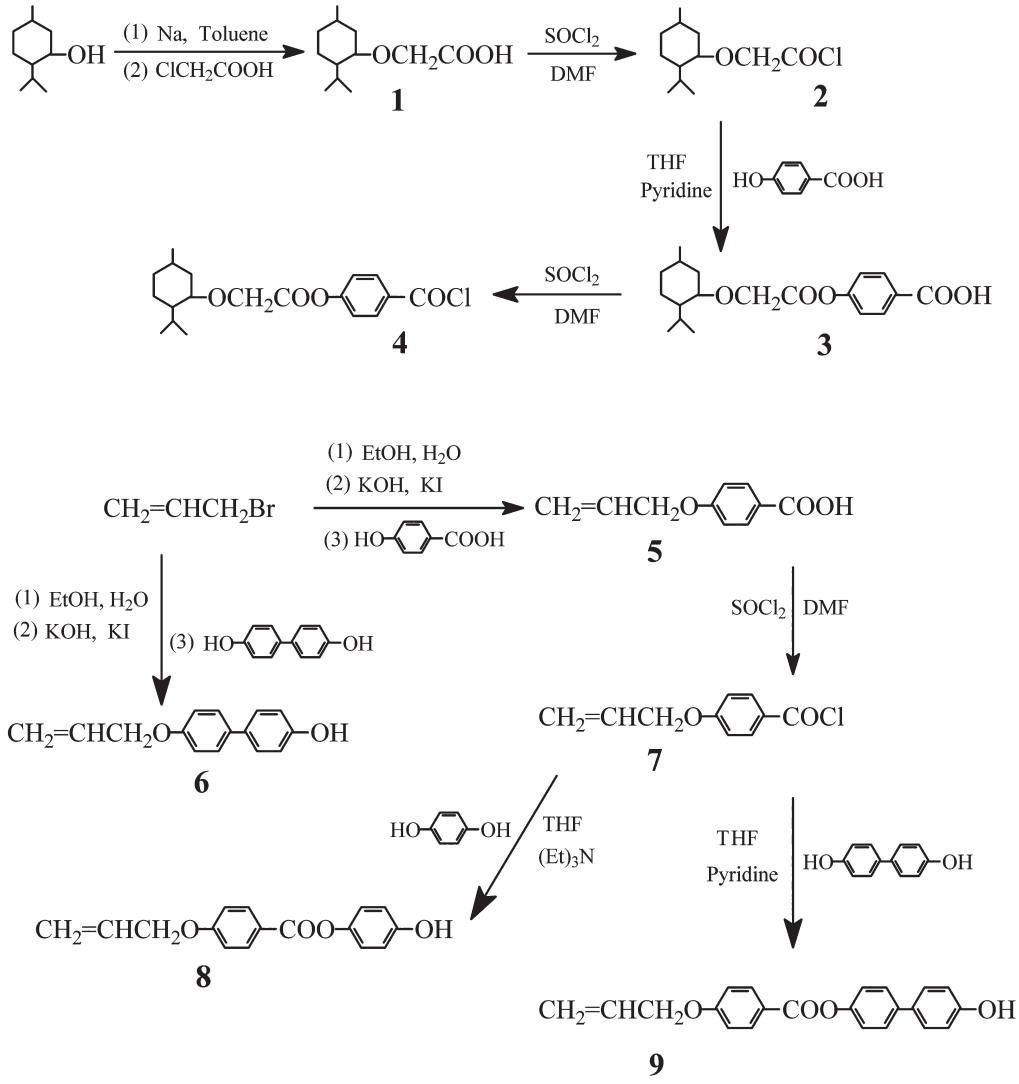

Scheme 1. Synthesis of intermediate compounds.

36 h, cooled to room temperature and then filtered. After the filtrate was concentrated, the crude product was precipitated by adding methanol to the filtrate, and then recrystallised from ethanol. Yield 65%. IR (KBr, cm^{-1}): 3076 (=C–H); 2955, 2850 (–CH_3, –CH_2–); 1779, 1721 (C=O); 1648 (C=C); 1607, 1512 (Ar–); 1253 (C–O–C). ^{1}H NMR ($CDCl_3$, TMS): δ 0.84–2.30 (m, 18H, menthyl–***H***); 3.27–3.32 (m, 1H,

Table 1. Yields, melting temperatures and IR characterisation of intermediate compounds.

Compound	Yield /%	Recrystallised solvent	T_m /°C	IR (KBr) /cm^{-1}
1	51	–	–	3500–2500 (–COOH); 2966, 2859 (CH_3–, –CH_2–); 1731, 1687 (C=O); 1211 (C–O–C)
3	85	80% ethanol	118	3500–2500 (–COOH); 2933, 2870 (CH_3–, –CH_2–); 1783, 1681 (C=O); 1603, 1506 (–Ar); 1204, (C–O–C)
5	65	ethanol	164	3300–2500 (–COOH); 1682 (C=O); 1644 (C=C); 1604, 1450 (–Ar); 1251 (C–O–C)
6	51	ethanol/acetone (2:1)	176	3401 (–OH); 1642 (C=C); 1609, 1512 (–Ar); 1246 (C–O–C)
8	87	ethanol	148	3421 (–OH); 1706 (C=O); 1643 (C=C); 1605, 1512 (–Ar); 1257 (C–O–C)
9	54	acetone	218	3445 (–OH); 1707 (C=O); 1645 (C=C); 1604, 1496 (–Ar); 1250 (C–O–C)

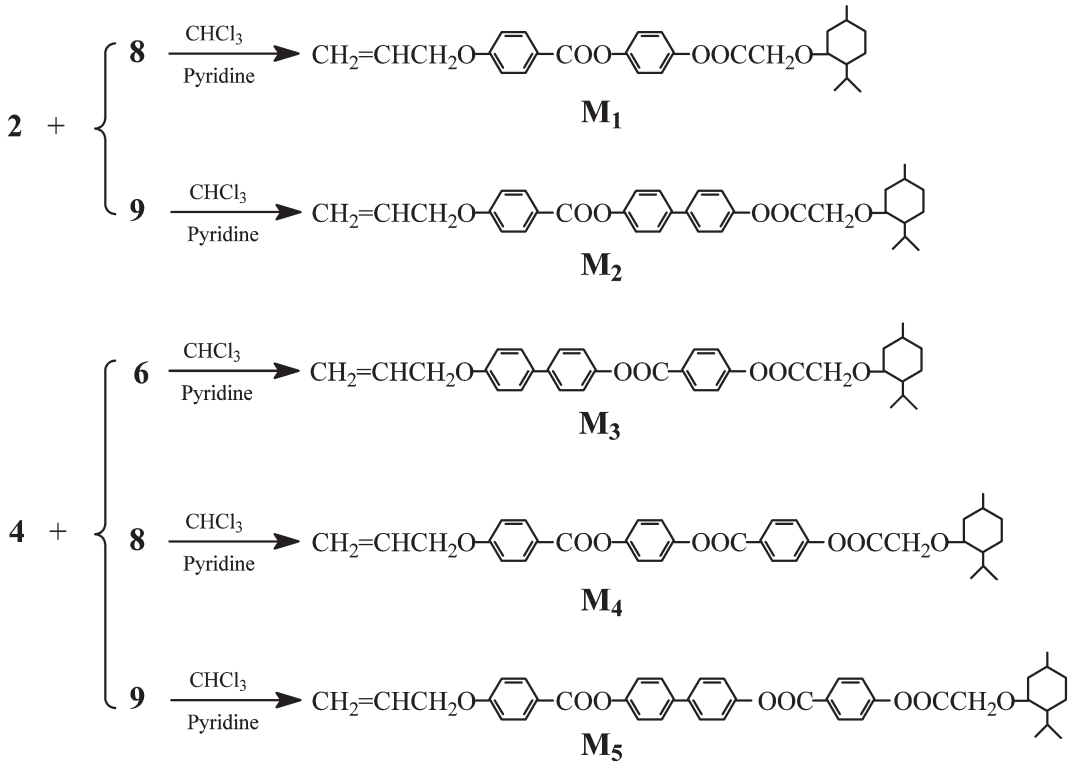

Scheme 2. Synthesis of chiral monomers.

–OOCCH$_2$OC***H***< in menthyl); 4.40–4.46 (m, 2H, –OOCC***H***$_2$O–); 4.64 (d, 2H, =CHC***H***$_2$O–); 5.32–5.50 (dd, 2H, C***H***$_2$=CH–); 6.05–6.11 (m, 1H, CH$_2$=C***H***–); 6.99–8.15(m, 8H, Ar–***H***).

*4-Allyloxybenzoyloxybiphenyl 4′-menthyloxyacetate (**M$_2$**).*

Recrystallised from ethanol/acetone (1:2). Yield 60%. IR (KBr, cm^{-1}): 3039 (=C–H); 2954, 2868 (–CH$_3$, –CH$_2$–); 1780, 1726 (C=O); 1650 (C=C); 1604, 1493 (Ar–); 1259 (C–O–C). ^{1}H NMR (CDCl$_3$, TMS): δ 0.85–2.34 (m, 18H, menthyl–***H***); 3.29–3.35 (m, 1H, –OOCCH$_2$OC***H***< in menthyl); 4.41–4.48 (m, 2H, –OOCC***H***$_2$O–); 4.66 (d, 2H, =CHC***H***$_2$O–); 5.35–5.51 (dd, 2H, C***H***$_2$=CH–); 6.06–6.15 (m, 1H, CH$_2$=C***H***–); 7.02–8.19(m, 12H, Ar–***H***).

*4-Allyloxybiphenyl 4′-menthyloxyacetyloxybenzoate (**M$_3$**).*

Recrystallised from ethanol/acetone (1:2). Yield 56%. IR (KBr, cm^{-1}): 3080 (=C–H); 2952, 2867 (–CH$_3$, –CH$_2$–); 1780, 1731 (C=O); 1646 (C=C); 1603, 1499 (Ar–); 1255 (C–O–C). ^{1}H NMR (CDCl$_3$, TMS): δ 0.85–2.37 (m, 18H, menthyl–***H***); 3.29–3.36 (m, 1H, –OOCCH$_2$OC***H***< in menthyl); 4.42–4.50 (m, 2H, –OOCC***H***$_2$O–); 4.64 (d, 2H, =CHC***H***$_2$O–); 5.34–5.52 (dd, 2H, C***H***$_2$=CH–); 6.07–6.13 (m, 1H, CH$_2$=C***H***–); 6.97–8.22(m, 12H, Ar–***H***).

*4-Allyloxybenzoyloxyphenyl 4′-menthyloxyacetyloxybenzoate (**M$_4$**).*

Recrystallised from ethanol/acetone (1:2). Yield 63%. IR (KBr, cm^{-1}): 3078 (=C–H); 2956, 2869 (–CH$_3$, –CH$_2$–); 1778, 1723 (C=O); 1650 (C=C); 1610, 1512 (Ar–); 1252 (C–O–C). ^{1}H NMR (CDCl$_3$, TMS): δ 0.86–2.39 (m, 18H, menthyl–***H***); 3.30–3.35 (m, 1H, –OOCCH$_2$OC***H***< in menthyl); 4.42–4.49 (m, 2H, –OOCC***H***$_2$O–); 4.67 (d, 2H, =CHC***H***$_2$O–); 5.36–5.55 (dd, 2H, C***H***$_2$=CH–); 6.07–6.14 (m, 1H, CH$_2$=C***H***–); 7.01–8.29(m, 12H, Ar–***H***).

*4-Allyloxybenzoyloxybiphenyl 4′-menthyloxyacetyloxybenzoate (**M$_5$**).*

Recrystallised from acetone. Yield 49%. IR (KBr, cm^{-1}): 3088 (=C–H); 2955, 2867 (–CH$_3$, –CH$_2$–); 1780, 1725 (C=O); 1649 (C=C); 1604, 1493 (Ar–); 1255 (C–O–C). ^{1}H NMR (CDCl$_3$, TMS): δ 0.85–2.38 (m, 18H, menthyl–***H***); 3.29–3.34 (m, 1H, –OOCCH$_2$OC***H***< in menthyl); 4.42–4.50 (m, 2H, –OOCC***H***$_2$O–); 4.66 (d, 2H, =CHC***H***$_2$O–); 5.34–5.53 (dd, 2H, C***H***$_2$=CH–); 6.05–6.15 (m, 1H, CH$_2$=C***H***–); 7.03–8.30(m, 12H, Ar–***H***).

Synthesis of the homopolymers

The synthetic route of the homopolymers $\mathbf{P_1}$–$\mathbf{P_5}$ is shown in Scheme 3. The synthesis of $\mathbf{P_1}$ is descibed as an example. $\mathbf{M_1}$ (5 mol % excess versus the Si–H groups in PMHS) and PMHS were dissolved in dry freshly distilled toluene. The reaction mixture was heated to 65°C under nitrogen and anhydrous conditions, and then 2 ml of THF solution with the H_2PtCl_6 catalyst (5 mg ml^{-1}) was injected into mixture with a syringe. The progress of the hydrosilylation reaction, monitored by the Si–H stretch intensity, went to completion, as indicated by IR spectra. $\mathbf{P_1}$ was obtained by precipitation from toluene solutions into methanol, purified by several filtrations from hot ethanol, and then dried in vacuo.

3. Results and discussion

Synthesis

The structures of target monomers were characterised by FT-IR and ^{1}H NMR spectroscopy. IR spectra of $\mathbf{M_1}$–$\mathbf{M_5}$ showed characteristic stretching bands at about 1779 cm^{-1} attributed to ester C=O in menthyloxyacetate, 1731–1721 cm^{-1} attributed to ester C=O in benzoate, 1651–1646 cm^{-1} attributed to olefinic C=C and 1610–1493 cm^{-1} attributed to aryl C=C. ^{1}H NMR spectra of $\mathbf{M_1}$–$\mathbf{M_5}$ showed multiplet at 8.30–6.97, 6.15–5.32 and 2.39–0.84 ppm corresponding to aryl protons, olefinic protons and methyl and methylene protons in menthyl, respectively. The ^{1}H NMR spectrum of $\mathbf{M_2}$ is shown as an example in Figure 1.

The homopolymers were synthesised through the hydrosilylation reaction. IR spectra of $\mathbf{P_1}$–$\mathbf{P_5}$ showed the complete disappearance of the Si–H stretching band at 2165 cm^{-1} and olefinic C=C stretching band at about 1651–1646 cm^{-1}. Characteristic Si–O and Si–C stretching bands appeared at 1300–1000 cm^{-1}. In addition, the absorption bands of ester C=O and aryl still existed.

Specific optical rotations

The specific optical rotations of the monomers $\mathbf{M_1}$–$\mathbf{M_5}$ and the corresponding homopolymers $\mathbf{P_1}$–$\mathbf{P_5}$ were evaluated at 22°C in toluene. The results are summarised in Tables 2 and 3. As shown in Tables 2 and 3, the specific optical rotations of $\mathbf{M_1}$–$\mathbf{M_5}$ and $\mathbf{P_1}$–$\mathbf{P_5}$ were all left-handed, which indicates

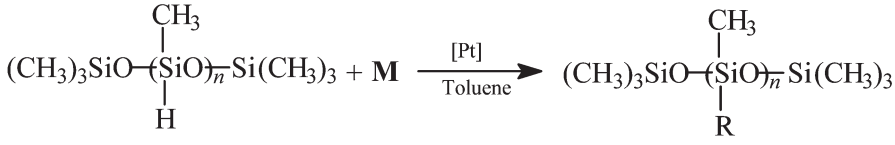

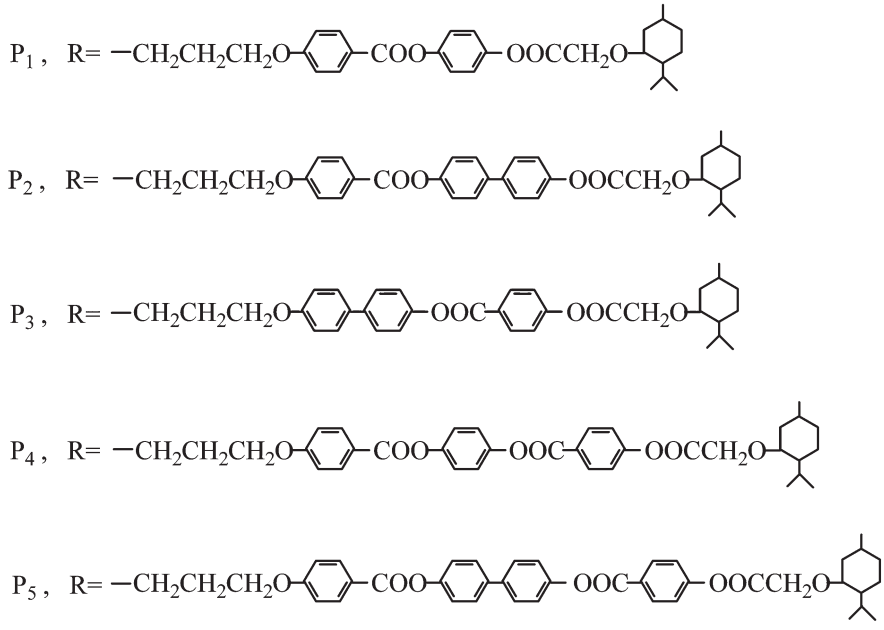

Scheme 3. Synthesis of chiral polymers.

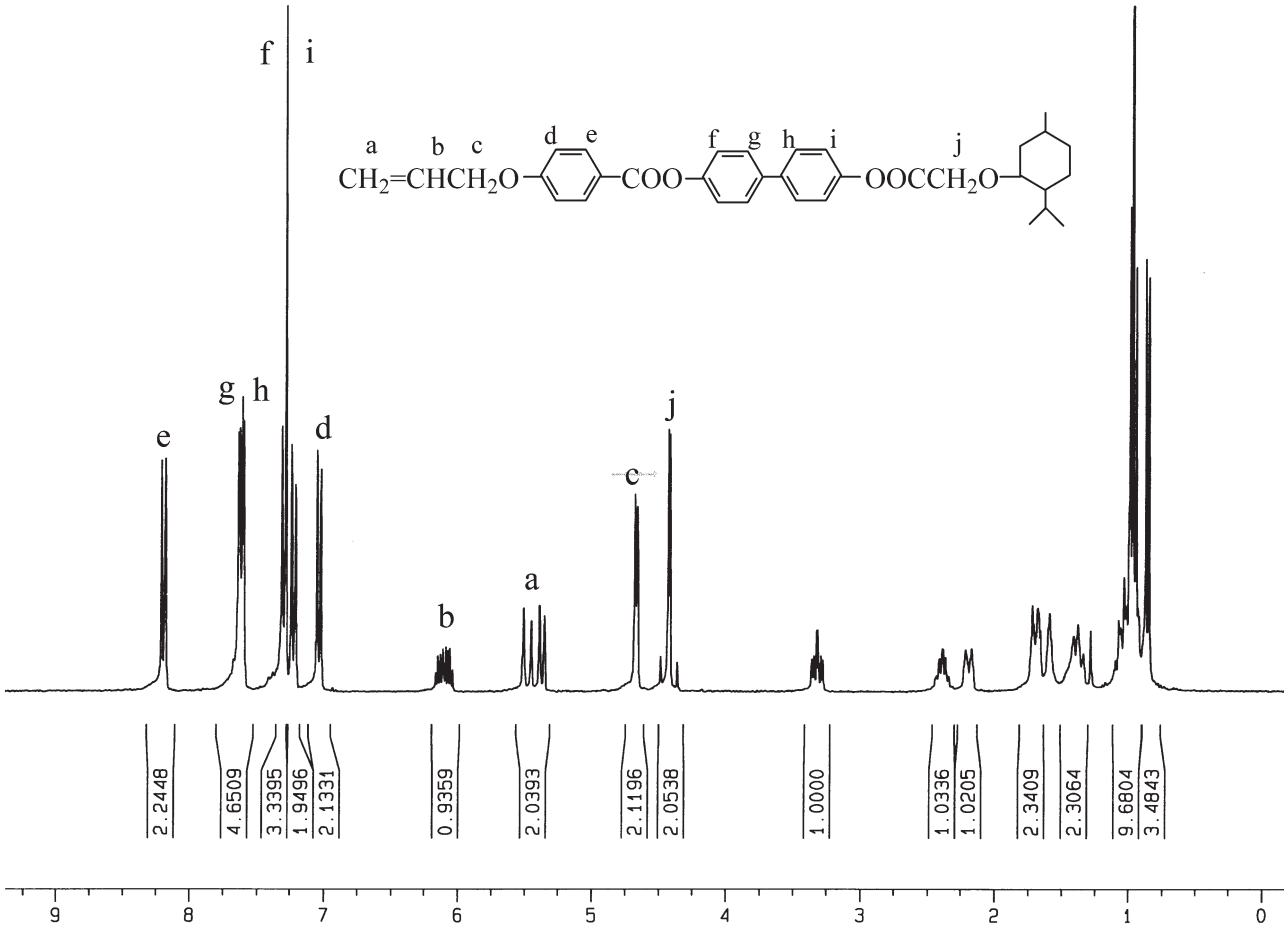

Figure 1. ^{1}H NMR spectrum of $\mathbf{M_2}$.

that the configuration or rotation direction of these chiral compounds is not affected by a series of chemical reaction or polymerisation. According to Table 2, the specific optical rotation value decreased with increasing the rigidity of mesogenic core. Compared with $\mathbf{M_1}$ ($[\alpha]_D^{22} = -49.9^\circ$), the monomers $\mathbf{M_2}$ and $\mathbf{M_5}$ with more aryl segments exhibited noticeably lower specific optical rotation values. The results suggest that the existence of high resonance biphenyl or more phenyl segment affects the polarity of the molecule, which is consistent with the result reported by Liu (*31*). Moreover, the specific optical rotation of $\mathbf{P_1}$–$\mathbf{P_5}$ displayed the same tendency as that described above for the corresponding monomers. In addition, the specific optical rotation value of $\mathbf{P_1}$–$\mathbf{P_5}$ was less than that of the corresponding monomers, which suggests that the polymerisation affects the molecular polarity.

Phase behaviour of the monomers

The phase behaviour of the monomers $\mathbf{M_1}$–$\mathbf{M_5}$ was investigated with DSC and POM. The phase transition temperatures, corresponding enthalpy changes

Table 2. Specific rotations and phase transition temperatures (°C) and enthalpies (J g^{-1}, in parentheses) of monomers studied.

Monomer	$[\alpha]_D^{22}$[a]	Phase transitions Heating Cooling	λ_m[c]	[d]Temp.
$\mathbf{M_1}$	−49.9	Cr 69.4 (45.6) I I 48.3 (40.3) Cr	—	—
$\mathbf{M_2}$	−41.7	Cr 101.5 (42.2) Ch 144.7 (1.4) I I 142.3 (0.7) Ch 77.2 (2.4) SmA 57.2 (23.2) Cr	412	103
$\mathbf{M_3}$	−43.5	Cr 120.4 (70.7) Ch 146.5 (1.5) I I 144.1 (1.0) Ch 97.0 (14.2) Cr	406	122
$\mathbf{M_4}$	−42.3	Cr 106.9 (48.8) Ch 161.9 (1.3) I I 159.8 (1.3) Ch 85.7 (39.7) Cr	397	108
$\mathbf{M_5}$	−33.7	Cr 147.5 (169.2) Ch 280.1[b] (-) D —	683	155

Cr=crystal, Ch=cholesteric, SmA=smectic A phase; I=isotropic; D=decomposition. [a]Specific optical rotation, 0.08 g in 25 ml toluene. [b]Temperature observed with POM. [c,d]Reflection wavelength measured by UV/visible spectroscopy at different temperature.

Table 3. Thermal and mesomorphic properties of polymers studied.

Polymer	$[\alpha]_D^{22}$	T_g /°C	T_i /°C	ΔT^b	T_d^c /°C	Mesophase
P₁	−49.5	16.8	–	–	313.2	–
P₂	−34.6	38.9	134.9	96.0	341.4	SmA
P₃	−36.5	44.1	135.3[a]	91.2	353.3	SmA
P₄	−40.7	43.5	147.2	103.7	332.9	SmA
P₅	−29.6	58.5	326.7[a]	268.2	346.5	SmA

[a]Temperature observed with POM. [b]Mesophase temperature range ($T_i - T_g$). [c]Temperature at which 5% weight loss occurred.

and mesophase types of **M₁–M₅**, obtained on the second heating and the first cooling scans, are summarised in Table 2. DSC thermograms of **M₂** and **M₄**, as examples, are shown in Figures 2 and 3.

DSC curves of **M₁** only showed a melting transition and a crystallisation transition on heating and cooling cycles. Moreover, POM observation showed that **M₁** did not exhibit any mesomorphic properties. For **M₂–M₄**, DSC heating thermograms not only showed a melting transition, but also a cholesteric to isotropic phase transition. On cooling, an isotropic to cholesteric phase transition and a crystallisation transition appeared. In addition, the DSC cooling curve of **M₂** also revealed a smectic A (SmA) phase transition between cholesteric and crystallisation phase transition, which is consistent with the POM result. For **M₅**, a melting transition was seen, and a cholesteric phase transition did not appear due to thermal decomposition. But POM observation confirmed that **M₅** showed the typical textures of a cholesteric phase.

As seen from the data listed in Table 2, the molecular structures had a considerable influence on the phase transition temperatures of **M₁–M₅**. **M₁** showed the melting temperature (T_m), but the isotropic or clearing temperature (T_i) did not appear because of the weaker rigidity of the mesogenic core. With increasing the rigidity of the mesogenic core or the number of aryl rings in monomer molecules, **M₂–M₅** showed not only T_m, but also T_i. Compared with the T_m of **M₁**, those of **M₂–M₅** increased by 32.1, 51.0, 37.5 and 78.1°C, respectively.

Taking the effect of the number of aryl rings on T_i into account, the equation derived by Dejeu is applicable (*36*):

$$T_i = \frac{0.084(\alpha_{//} - \alpha_{\perp})I}{KV^2}, \quad (1)$$

where K is Boltzman's constant, I is ionised electric potential, V is molar volume and $\alpha_{//}-\alpha_{\perp}$ is the polarisability anisotropy between directions parallel and normal to the molecular axis. In the conjugate system of the aryl rings, the $\alpha_{//}$ value is very great, so the $\alpha_{//}$ value will increase with increasing number of the aryl rings, and T_i also increases. For example, compared with the T_i of **M₄**, that of **M₅** is increased by 118.2°C.

For **M₂** and **M₃**, although their molecular formula is completely the same and, moreover, they were synthesised with the same materials and reagents, their molecular arrangement and structures are different, so

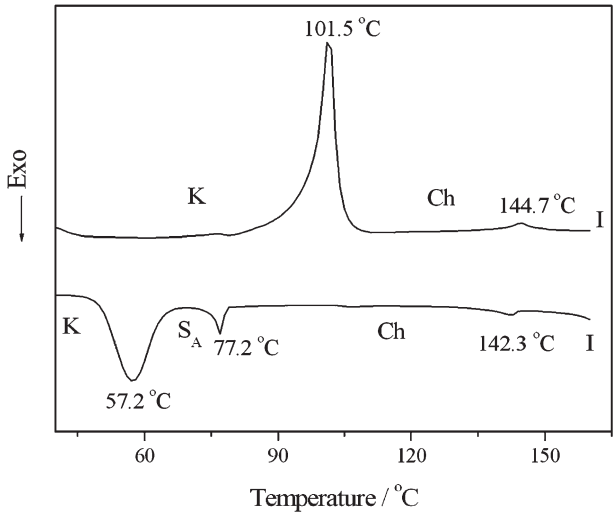

Figure 2. DSC thermograms of **M₂**.

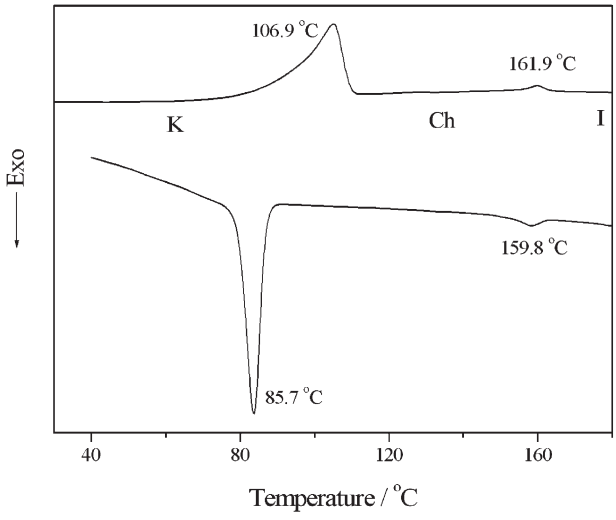

Figure 3. DSC thermograms of **M₄**.

their phase behaviour and LC properties were also different: (i) **M2** showed an enantiotropic cholesteric phase and a monotropic SmA phase, whereas **M3** showed only an enantiotropic cholesteric phase; (ii) T_m of **M2** was 101.5°C, whereas that of **M3** was 120.4°C, i.e. their T_m values were noticeably different. However, T_i values of **M2** and **M3** showed hardly any difference. Although the molecular structures of **M2** and **M3** are different, they are made up of the same constituent and aryl units. According to equation (1), T_i of **M2** and **M3** should be nearly same.

The bridge bond in the aryl rings had an influence on the phase transition temperatures because the conjugation action of the ester bridge bond. According to Table 2, T_m and T_i of **M4** increased by 5.4 and 17.2°C compared with those of **M2**.

Optical properties and textures of the monomers

The unique optical properties of cholesteric LC materials are related to their helical supermolecular structure. The periodic helical structure of cholesteric phase selectively reflects visible light like an ordinary diffraction grating, the pitch of which controls the wavelength of selective reflection of light. If the reflected wavelength lies in the visible range of the spectrum, the cholesteric phase exhibits brilliant colours. The wavelength of selective reflection of light, λ_m, obeys the Bragg condition:

$$\lambda_m = \boldsymbol{n}P\cos\theta, \tag{2}$$

where $\bar{n}$ is the average index of refraction, P is the pitch of the cholesteric phase, defined as the spatial distance over which the director rotates 360°, and θ is the incidence angle.

It is known that the pitch and the reflection wavelength depend on the molecular structure, such as the polymer backbone, the rigidity of mesogenic core, the flexible spacer length and external conditions (such as temperature, force, electric and magnetic fields, etc). For **M2**–**M5**, the rigidity of mesogenic core not only affected the phase transition temperatures, but also the selective reflection wavelength of cholesteric phase. The maximum reflection wavelength (normal incidence) λ_m of **M2**–**M5**, summarised in Table 2, was measured by UV–visible spectroscopy with hot stage at cholesteric phase. According to Table 2, the selective reflection of light shifted to the long wavelength region with increasing rigidity of the mesogenic core. The reflection colour of **M2**–**M4** exhibited violet at 103, 122 and 108°C, respectively, and that of **M5** showed red at 155°C and yellow at 263°C (normal observation). Moreover, the selective reflection of **M2**–**M5** shifted to the short wavelength region with increasing temperature, so λ_m was temperature dependent. According to equation (2), an increase of the reflection angle made the selective reflection of light shift to the short wavelength region.

In addition, the helical pitch not only affects the selective reflection wavelength and colour, but also is related to texture type of cholesteric phase. In general, cholesteric LCs at zero field exhibit two optically contrasting stable states: planar (including oily streak and Grandjean) texture and focal conic texture. We found that: (1) if a cholesteric phase has a shorter pitch length, the texture of blue phase or focal conic texture is usually observed; (2) if a pitch length of cholesteric phase lies in the visible range of the spectrum, the planar, oily streak or Grandjean textures are usually observed; (3) if a cholesteric phase has a longer pitch length than the wavelength of visible light, the finger print texture is usually observed.

POM results showed that **M2**–**M5** exhibited enantiotropic cholesteric oily streak texture and focal conic texture on heating and cooling cycles. In addition, **M2** also exhibited fan shaped texture of a SmA phase, and **M4** also revealed platelet texture of a cubic blue phase (BP) on cooling to 160.2°C from the isotropic melt. The different colours of the BP correspond to different lattice planes, which show Bragg scattering at different wavelengths. Further cooling to 158.9°C, the platelet texture of cubic BP began to transform to the focal conic texture of the cholesteric phase. The optical textures of **M4**, as examples, are shown in Figure 4.

Phase behaviour and mesomorphic properties of the polymers

The phase behaviour and mesomorphic properties of polymers **P1**–**P5** were studied with DSC, TGA, POM and XRD. Their phase transition temperatures, thermal decomposition temperature and mesophase types obtained are summarised in Table 3. DSC curves of **P1**, **P3** and **P5** only showed the glass transition, but POM results showed that **P3** and **P5** exhibited the mesomorphic properties. DSC thermograms of **P2** and **P4** showed a glass transition at low temperature and a LC to isotropic phase transition at high temperature.

In general, the phase behaviour and mesomorphic properties of side-chain LCPs mainly depend on the polymer backbone, the mesogenic units, and the flexible spacer. For **P1**–**P5**, because of the same polymer backbone and length of the flexible spacer in the side groups, the corresponding phase transition temperatures mainly depend on the rigidity of the

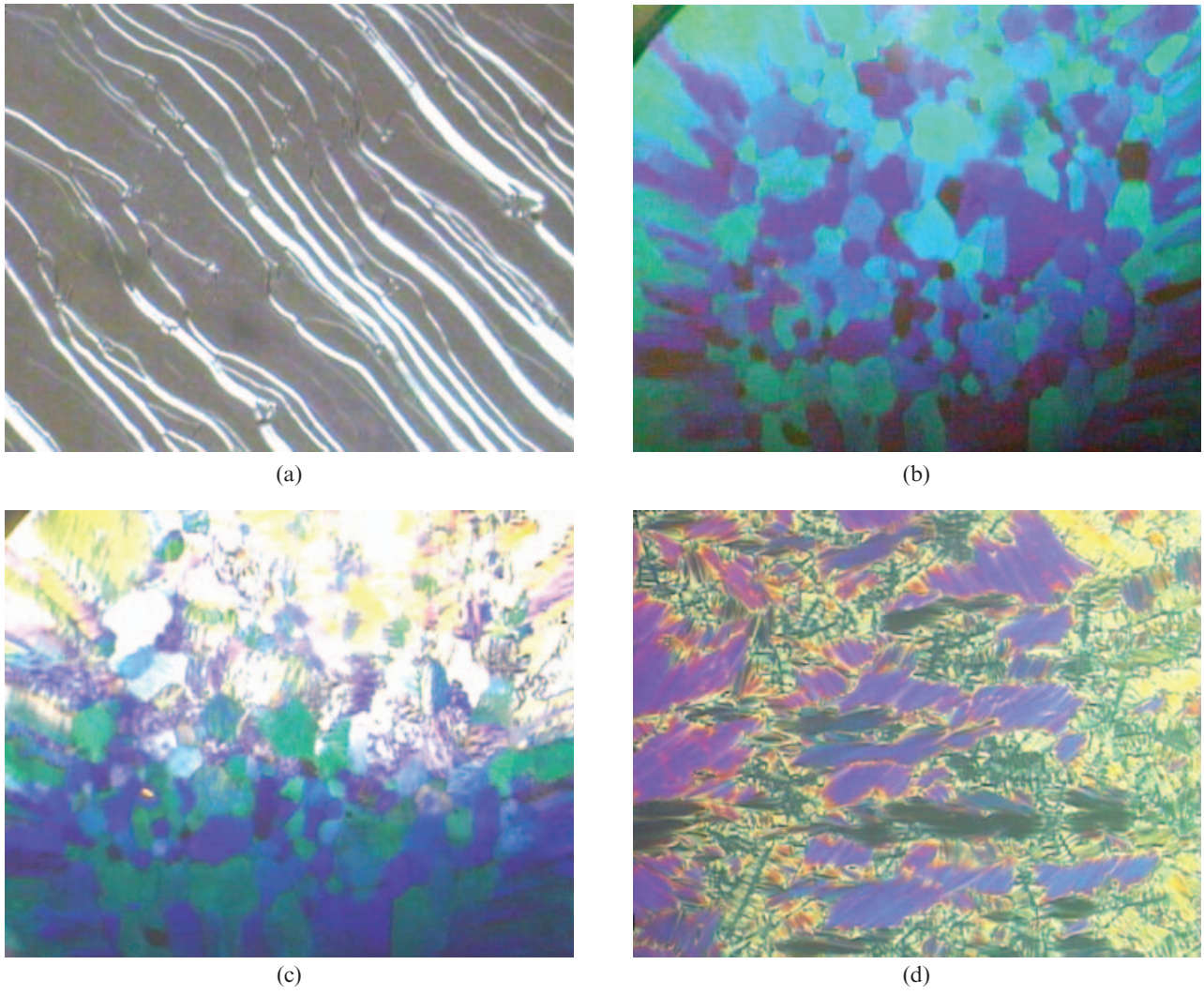

Figure 4. Optical textures of **M$_4$** (200 ×): (a) oily streak texture of cholesteric phase on heating to 142.3°C; (b) platelet texture of cubic blue phase on cooling to 159.0°C; (c) platelet texture of blue phase growing into focal conic texture of cholesteric phase on cooling to 158.5°C; (d) focal conic texture of cholesteric phase on cooling to 153.1°C.

mesogenic unit. The glass transition temperature (T_g) and T_i of LCPs are a very important parameter in connection with structures and properties. According to Table 3, with increasing rigidity of the mesogenic units, T_g and T_i increased, and ΔT also widened because T_i increased more than T_g. Compared with T_g of **P$_1$**, that of **P$_2$** and **P$_5$** increased by 22.1 and 41.7°C, respectively. Moreover, T_i increased from 134.9°C for **P$_2$** to 326.7°C for **P$_5$**, and ΔT increased from 96.0°C for **P$_2$** to 268.2°C for **P$_5$**. For **P$_2$**–**P$_4$**, their T_g and T_i did not remarkably change because of the almost same rigidity of mesogenic units.

The thermal stability of **P$_1$**–**P$_5$** was detected with TGA. The corresponding data are shown in Table 3. Representative TGA curves of **P$_2$** and **P$_4$** are shown in Figure 5. TGA results showed that the temperatures at which 5% weight loss occurred (T_d) were

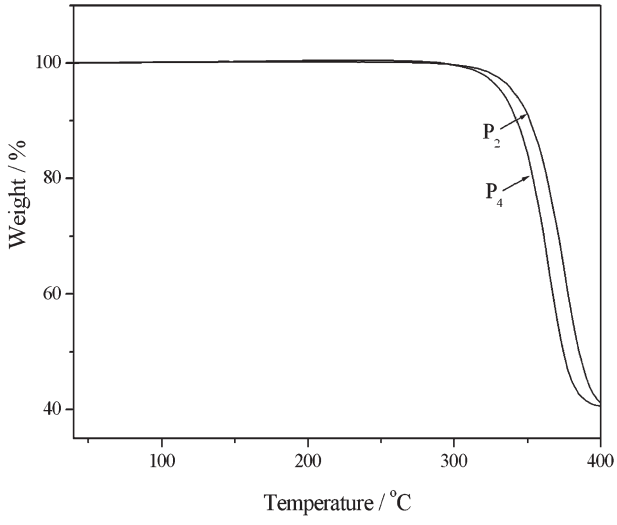

Figure 5. TGA curves of **P$_2$** and **P$_4$**.

greater than 310°C for $\mathbf{P_1}$–$\mathbf{P_5}$; this indicates that these homopolymers had good thermal stability.

POM results showed that $\mathbf{P_2}$–$\mathbf{P_5}$ exhibited the fan shaped textures of the SmA phase; in this case the smectic layers are basically perpendicular to the substrate plane. However, the cholesteric phase, exhibited for their corresponding monomers, did not appear. This indicates that the polymer chains hinder the formation of cholesteric helical supermolecular structure of the mesogens, and the mesogenic moieties are ordered in a smectic orientation with their centres of gravity in plane. It is also noted that the mesophase formed by side-chain LCPs is more organised than that exhibited by the corresponding monomers. This behaviour is attributed to an increased density of the mesogenic polymer and hence an easier organisation into the LC phases. Moreover, the LCPs with siloxane macromolecular chains tend to form lower order smectic phases.

XRD studies were carried out to obtain more detailed information on the mesomorphic structure and type. In general, a sharp and strong peak associated with the smectic layers at small angle and a broad peak associated with lateral packing at wide angle can be observed for smectic structure. For $\mathbf{P_2}$–$\mathbf{P_5}$, XRD confirmed the presence of the SmA phase structure. Their X-ray patterns all exhibited a sharp and strong reflection at small angle region. Figure 6 shows the small-angle XRD curves of $\mathbf{P_2}$ and $\mathbf{P_4}$ mesophases. The *d*-spacing of the first-order reflections was 20.9 and 23.1 Å, respectively. When the temperature decreased in the mesophase, the *d*-spacing of the first-order reflection hardly changed. This gives strong evidence for the formation of the SmA phase. This result is also in consistent with POM results.

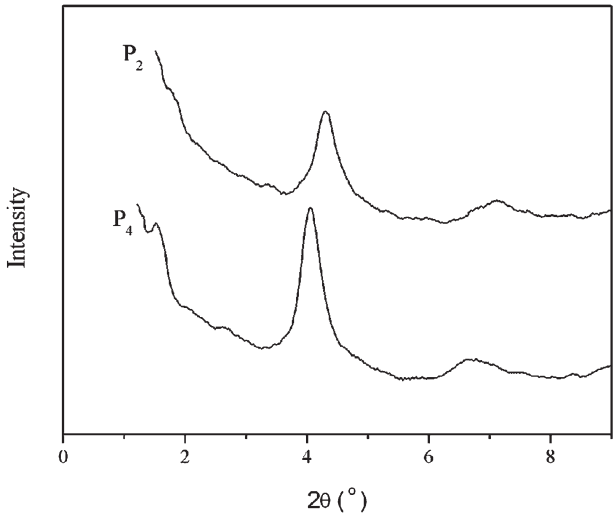

Figure 6. Small-angle XRD patterns of $\mathbf{P_2}$ and $\mathbf{P_4}$.

4. Conclusions

Four new cholesteric monomers ($\mathbf{M_2}$–$\mathbf{M_5}$), and their corresponding side-chain smectic homopolymers ($\mathbf{P_2}$–$\mathbf{P_5}$), based on mesogenic menthyl groups were synthesised and characterised. The monomers and homopolymers obtained with more aryl segments exhibited obviously lower specific optical rotation values. $\mathbf{M_1}$ and $\mathbf{P_1}$ did not show LC properties. $\mathbf{M_2}$–$\mathbf{M_5}$ exhibited cholesteric oily streak texture and focal conic texture. Moreover, $\mathbf{M_2}$ also exhibited the fan shaped texture of a SmA phase, and $\mathbf{M_4}$ revealed the platelet texture of a cubic BP on cooling cycle. The selective reflection of light shifted to the long wavelength region with increasing the rigidity of mesogenic core for $\mathbf{M_2}$–$\mathbf{M_5}$. $\mathbf{P_2}$–$\mathbf{P_5}$ all exhibited the fan-shaped textures of the SmA phase. In addition, with increasing rigidity of the mesogenic core, the corresponding T_m or T_g and T_i increased, and ΔT widened. T_m or T_g and T_i of the monomers and polymers with almost same rigidity of mesogenic units did not remarkably change. All of the obtained homopolymers displayed very good thermal stability.

Acknowledgements

The authors are grateful to National Natural Science Foundation of China, Program for New Century Excellent Talents (NCET) in University, and Natural Science Foundation of Liaoning Province for financial support of this work.

References

(1) Broer D.J.; Lub J.; Mol G.N. *Nature* **1995**, *378*, 467–469.
(2) Pfeuffer T.; Strohriegl P. *Macromol. Chem. Phys.* **1999**, *200*, 2480–2486.
(3) Bacilieri A.; Caruso U.; Panunzi B.; Roviello A.; Sirigu A. *Polymer* **2000**, *41*, 6423–6430.
(4) Zheng S.J.; Li Z.F.; Zhang S.Y.; Cao S.K.; Guo K.; Zhou Q.F. *Polym. Adv. Technol.* **2000**, *11*, 219–227.
(5) Shibaev P.V.; Kopp V.I.; Genack A.Z. *J. Phys. Chem.* B **2003**, *107*, 6961–6964.
(6) Zhang B.; Hu J.; Yao D.; Zhang L. *Acta Polym. Sin.* **2003**, *6*, 799–802.
(7) Oaki Y.; Imai H. *J. Am. Chem. Soc.* **2004**, *126*, 9271–9275.
(8) Abraham S.; Paul S.; Narayan G.; Prasad S.K.; Rao D.S.S. *Adv. Funct. Mater.* **2005**, *15*, 1579–1584.
(9) Gomar-Nadal E.; Veciana J.; Rovira C.; Amabilino D.B. *Adv. Mater.* **2005**, *17*, 2095–2098.
(10) Brettar J.; Burgi T.; Donnio B.; Guillon D.; Klappert R.; Scharf T.; Deschenaux R. *Adv. Funct. Mater.* **2006**, *16*, 260–267.
(11) Hsiue G.H.; Lee R.H. *J. Polym. Sci. B* **2006**, *44*, 2035–2049.

(12) Ohta R.; Togashi F.; Goto H. *Macromolecules* **2007**, *40*, 5228–5230.
(13) Zhang B.Y.; Hu J.S.; Zang B.L.; Zhou A.J. *J. Appl. Polym. Sci.* **2003**, *88*, 1936–1941.
(14) Hu J.S.; Zhang B.Y.; He X.Z.; Cheng C.S. *Liq. Cryst.* **2004**, *31*, 1357–1365.
(15) Hsiue G.H.; Chen J.H. *Macromolecules* **1995**, *28*, 4366–4376.
(16) Hsu C.S.; Chu P.H.; Chang H.L.; Hsieh T.H. *J. Polym. Sci. A* **1997**, *35*, 2793–2800.
(17) Mihara T.; Nomura K.; Funaki K.; Koide N. *Polym. J.* **1997**, *29*, 303–308.
(18) Hu J.S.; Zhang B.Y.; Zhou A.J.; Du B.G.; Yang L.Q. *J. Appl. Polym. Sci.* **2006**, *100*, 4234–4239.
(19) Soltysiak J.T.; Czuprynski K.; Drzewinski W. *Polym. Int.* **2006**, *55*, 273–278.
(20) Zheng Z.; Sun Y.Y.; Xu J.; Chen B.; Su Z.Q.; Zhang Q.J. *Polym. Int.* **2007**, *56*, 699–706.
(21) Zhang B.Y.; Hu J.S.; Yang L.Q.; He X.Z.; Liu C. *Eur. Polym. J.* **2007**, *43*, 2017–2027.
(22) Mihara T.; Nomura K.; Funaki K. *Polym. J.* **1997**, *29*, 309–315.
(23) Altomare A.; Andruzzi L.; Ciardelli F.; Gallot B.; Solaro1 R. *Polym. Int.* **1998**, *47*, 419–427.
(24) Bobrovsky A.Y.; Boiko N.I.; Shibaev V.P. *Liq. Cryst.* **1998**, *24*, 489–500.
(25) Bobrovsky A.Y.; Boiko N.I.; Shibaev V.P.; Wolff D.; Springer J. *Macromolecules* **1998**, *31*, 5800–5804.
(26) Bobrovsky A.Y.; Boiko N.I.; Shibaev V.P. *Ferroelectrics* **1998**, *212*, 387–394.
(27) Bobrovsky A.Y.; Shibaev V.P. *Adv. Funct. Mater.* **2002**, *12*, 367–372.
(28) Lee Y.K.; Onimura K.; Tsutsumi H.; Oishi T. *J. Polym. Sci. A* **2000**, *38*, 4315–4325.
(29) Hu J.S.; Zhang B.Y.; Pan W.; Zhou A.J. *Liq. Cryst.* **2005**, *32*, 441–447.
(30) Du B.G.; Hu J.S.; Zhang B.Y.; Xiao L.J.; Wei K.Q. *J. Appl. Polym. Sci.* **2006**, *102*, 5559–5565.
(31) Liu J.H.; Yang P.C. *Polymer* **2006**, *47*, 4925–4935.
(32) Liu J.H.; Yang P.C.; Hung H.J. *Liq. Cryst.* **2007**, *34*, 891–902.
(33) Lin H.S.; Deng Y.N. *Chin. J. Pharm.* **1998**, *28*, 184–185.
(34) Hu J.S.; Zhang B.Y.; Feng Z.L.; Wang H.G.; Zhou A.J. *J. Appl. Polym. Sci.* **2001**, *80*, 2335–2340.
(35) Hu J.S.; Ren S.C.; Zhang B.Y. *J. Appl. Polym. Sci.* **2008**, *109*, 2187–2194.
(36) Dejeu W.H. *Mol. Cryst. Lig. Cryst.* **1977**, *40*, 1–6.